A Numerical Study of Firebrands Scattering in Urban Fire Based on CFD and Firebrands Aerodynamics Measurements

HONG HUANG,* RYOZO OOKA AND SHINSUKE KATO

Institute of Industrial Science, The University of Tokyo, 4-6-1 Komaba Meguro-ku, Tokyo, 153-8505, Japan

YOSHIHIKO HAYASHI

Building Research Institute, 1 Tachihara, Tsukuba, Ibaraki, 305-0802, Japan

(Received July 15, 2006)

ABSTRACT: Firebrands are found to be an important factor in the spread of large urban fire. In this study, in order to predict the scattering of firebrands in an urban fire, a computational fluid dynamics (CFD), turbulent combustion model, radiation model, and firebrand scattering model are coupled and it is validated by a fire wind tunnel experiment. The density, terminal velocity, and Stokes diameters of firebrands which are necessary for the firebrand scattering model are measured. The ratio of Stokes diameter to equivalent diameter is focused on 0.2–0.7. An urban fire simulation in a modeled urban area has been conducted using the coupled model and the firebrand experimental data. It is found that when the inflow wind velocity is comparatively slow, the size of the thermal plume becomes significant, and when the inflow wind velocity is high, the thermal plume is suppressed and greatly inclines to the leeward side, which increases the risk of the fire spreading to neighboring buildings. Firebrands can be scattered over 400 m. Firebrands are blown up by the thermal plume and the scattering distances are influenced by the background flow field, the magnitude of thermal plume, and the Stokes diameters of firebrands.

*Author to whom correspondence should be addressed. E-mail: hhong@iis.u-tokyo.ac.jp
Figures 1 and 3–8 appear in color online: http://jfs.sagepub.com

0734-9041/07/04 0355–24 $10.00/0 DOI: 10.1177/0734904107073008

KEY WORDS: firebrands, urban fire, CFD, aerodynamics measurement.

INTRODUCTION

THE FACTORS THAT can cause fire spread are contact fire, radiation, convection, firebrands, etc. which are shown in Figure 1. From investigations of past urban fires, fire spread by firebrands almost occurred, especially in the case of fires that cause extensive damage [1,2]. However, there are few findings on the properties and mechanisms of firebrands because there are many uncertain factors, such as meteorological conditions, the combustion conditions in the building that is on fire, the types of building materials, etc. Shiraishi et al. [3] simulated firebrand scattering in urban fires using computational fluid dynamics (CFD). In their study, firebrands are treated as airborne particles. This assumption holds for small-diameter firebrands; however, for large-diameter firebrands, a different treatment is necessary. Some simulations [4–6] about firebrand scattering has been done considering the gravity and drag force of firebrands and compared with investigation results; however, the fluid dynamics properties of firebrands, such as density and Stokes diameter are not clarified, which are very important for the prediction of firebrand scattering.

In this study, in order to predict urban fire and firebrand scattering, a CFD, turbulent combustion model, radiation model, and firebrand scattering model are coupled. Then, the density, terminal velocity, and Stokes diameters of firebrands which are necessary for the firebrand scattering model are measured. Finally, an urban fire simulation in a modeled urban area has been conducted using the coupled model and the firebrand experimental data. The firebrands scattering model used here focuses on the flying of firebrands and the combustion time of firebrands is thought to be much longer than the flying time. It is also assumed that the temperature of firebrands gives no influence on the air flow, and the mass and shape are not changed during flight.

MODEL DESCRIPTION

The CFD Model

Both the density and the temperature in the fire plume fluctuate widely. Therefore, the assumption of an incompressible fluid (Boussinesq approximation) does not hold, and the plume must be considered as a compressible fluid. Thus, the Favre-averaged process is introduced here for all transport equations. Table 1 shows the governing equations.

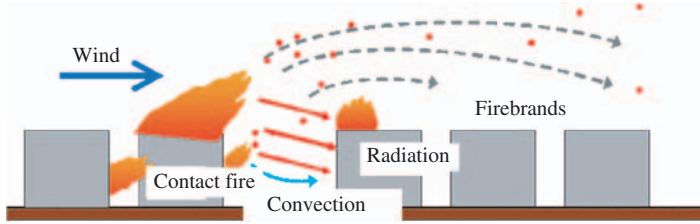

Figure 1. Urban fire spread process.

Table 1. Governing equations.

$$\frac{\partial \bar{\rho}}{\partial t} + \frac{\partial (\bar{\rho}\tilde{u}_j)}{\partial x_j} = 0 \tag{1}$$

$$\frac{\partial (\bar{\rho}\tilde{u}_i)}{\partial t} + \frac{\partial}{\partial x_j}(\bar{\rho}\tilde{u}_i\tilde{u}_j) = -\frac{\partial \bar{p}}{\partial x_i} + \frac{\partial}{\partial x_j}(\bar{\tau}_{ij} - \bar{\rho}\widetilde{u_i''u_j''}) + \bar{\rho}g_i \tag{2}$$

$$\frac{\partial (\bar{\rho}\tilde{h})}{\partial t} + \frac{\partial}{\partial x_j}(\bar{\rho}\tilde{u}_j\tilde{h}) = \frac{\partial \bar{p}}{\partial t} + \frac{\partial}{\partial x_j}\left(\frac{\lambda}{c_p}\frac{\partial \tilde{h}}{\partial x_j} - \bar{\rho}\widetilde{u_i''h_j''} + \sum_{n=1}^{N}\bar{h}_n\bar{\rho}D_n\frac{\partial \tilde{Y}_n}{\partial x_j}\right) + \bar{u}_j\frac{\partial \bar{p}}{\partial x_j} + \bar{\tau}_{ij}\frac{\partial \bar{u}_i}{\partial x_j} - \bar{S}_R \tag{3}$$

$$\frac{\partial (\bar{\rho}\tilde{Y}_n)}{\partial t} + \frac{\partial}{\partial x_j}(\bar{\rho}\tilde{u}_j\tilde{Y}_n) = \frac{\partial}{\partial x_j}\left(\bar{\rho}D_n\frac{\partial \tilde{Y}_n}{\partial x_j} - \bar{\rho}\widetilde{u_i''Y_n''}\right) + \bar{w}_n \tag{4}$$

$$\frac{\partial (\bar{\rho}\tilde{k})}{\partial t} + \frac{\partial (\bar{\rho}\tilde{u}_j\tilde{k})}{\partial x_j} = \frac{\partial}{\partial x_j}\left(\left(\mu + \frac{\mu_t}{\sigma_k}\right)\frac{\partial \tilde{k}}{\partial x_j}\right) + \mu_t\left(\frac{\partial \tilde{u}_i}{\partial x_j} + \frac{\partial \tilde{u}_j}{\partial x_i}\right)\frac{\partial \tilde{u}_i}{\partial x_j} - \frac{2}{3}\left(\mu_t\frac{\partial \tilde{u}_k}{\partial x_k} + \bar{\rho}\tilde{k}\right)\frac{\partial \tilde{u}_i}{\partial x_i} - g_i\frac{\mu_t}{\sigma_h}\frac{1}{\bar{\rho}}\frac{\partial \bar{\rho}}{\partial x_i} - \bar{\rho}\tilde{\varepsilon} \tag{5}$$

(*continued*)

Table 1. Continued.

$$\frac{\partial(\bar{\rho}\tilde{\varepsilon})}{\partial t}+\frac{\partial(\bar{\rho}\tilde{u}_j\tilde{\varepsilon})}{\partial x_j}=\frac{\partial}{\partial x_j}\left(\left(\mu+\frac{\mu_t}{\sigma_\varepsilon}\right)\frac{\partial\tilde{\varepsilon}}{\partial x_j}\right)$$
$$+C_{\varepsilon1}\frac{\tilde{\varepsilon}}{\tilde{k}}\left(\mu_t\left(\frac{\partial\tilde{u}_i}{\partial x_j}+\frac{\partial\tilde{u}_j}{\partial x_i}\right)\frac{\partial\tilde{u}_i}{\partial x_j}\right.$$
$$-\frac{2}{3}\left(\mu_t\frac{\partial\tilde{u}_k}{\partial x_k}+\bar{\rho}\tilde{k}\right)\frac{\partial\tilde{u}_i}{\partial x_i}$$
$$\left.+C_{\varepsilon3}\max\left(-g_i\frac{\mu_t}{\sigma_h}\frac{1}{\bar{\rho}}\frac{\partial\bar{\rho}}{\partial x_i},0\right)\right)$$
$$-C_{\varepsilon2}\bar{\rho}\frac{\tilde{\varepsilon}^2}{\tilde{k}}+C_{\varepsilon4}\bar{\rho}\tilde{\varepsilon}\frac{\partial\tilde{u}_i}{\partial x_i} \tag{6}$$

$$h=\sum_{n=1}^{N}Y_nh_n=\sum_{n=1}^{N}Y_n\left(h_{0,n}+\int_{T_0}^{T}c_{p,n}dT\right) \tag{7}$$

$$\bar{\rho}=\frac{\bar{p}}{R\sum_{n=1}^{N}(\tilde{T}\tilde{Y}_n/M_n)} \tag{8}$$

$$\bar{\tau}_{ij}=\mu\left(\frac{\partial\bar{u}_i}{\partial x_j}+\frac{\partial\bar{u}_j}{\partial x_i}-\frac{2}{3}\frac{\partial\bar{u}_k}{\partial x_k}\delta_{ij}\right) \tag{9}$$

$$\bar{\rho}\widetilde{u_i''u_j''}=-\mu_t\left(\frac{\partial\tilde{u}_i}{\partial x_j}+\frac{\partial\tilde{u}_j}{\partial x_i}\right)+\frac{2}{3}\left(\mu_t\frac{\partial\tilde{u}_k}{\partial x_k}+\bar{\rho}\tilde{k}\right)\delta_{ij} \tag{10}$$

$$\bar{\rho}\widetilde{u_j''h''}=-\frac{\mu_t}{\sigma_h}\frac{\partial\tilde{h}}{\partial x_j} \tag{11}$$

$$\bar{\rho}\widetilde{u_j''Y_n''}=-\frac{\mu_t}{\sigma_n}\frac{\partial\tilde{Y}_n}{\partial x_j} \tag{12}$$

$$\sigma_k=1.0,\quad \sigma_\varepsilon=1.22,\quad \sigma_h=0.7,\quad \sigma_n=0.7,$$
$$C_{\varepsilon1}=1.44,\quad C_{\varepsilon2}=1.92,\quad C_{\varepsilon3}=1.0,\quad C_{\varepsilon4}=-0.33$$
$$n=\text{fuel, oxygen, product}$$

A modified $k-\varepsilon$ model, as proposed by El Tahry [7] for compressible reciprocating engine flows, is used. The main difference between the modified model and the standard model is the last term in the ε equation (Equation (6)) which results from the effects of compressibility.

A fire model is required to close the above governing equations. One of the common methods is to replace the fire region by a volumetric heat source (or sometimes heat flux). However, a combustion model that accounts for the chemical reactions between fuel and oxygen must be included to describe the actual fire more closely. Therefore, combustion in the gaseous phase is modeled using the eddy dissipation combustion model [8] here, which is widely used in fire modeling [9]. The chemical reaction rate is proportional to the turbulence eddy decay rate and minimum concentration of the fuel or oxygen:

$$\bar{w}_f = -\bar{\rho}\left(\frac{\varepsilon}{k}\right)\min\left(A\tilde{Y}_f, A\tilde{Y}_{O_2}/i\right) \tag{13}$$

where A takes the value 4.0, and i is the stoichiometric ratio of oxygen to fuel. The following chemical reaction is assumed [10]:

$$\begin{aligned} \mathrm{C}_n\mathrm{H}_m + \left(n - s + \frac{m}{4}\right)(\mathrm{O}_2 + 3.76\mathrm{N}_2) \rightarrow s\mathrm{C} + (n-s)\mathrm{CO}_2 \\ + \frac{m}{2}\mathrm{H}_2\mathrm{O} + 3.76\left(n - s + \frac{m}{4}\right)\mathrm{N}_2 \end{aligned} \tag{14}$$

Here s is a parameter that defines the amount of soot produced. A zero value means complete combustion reaction is obtained to give carbon dioxide and water. When s is non-zero in Equation (14), some of the carbon remains as soot, with a consequent reaction to finally become CO_2. The value of s can be decided from the soot conversion factor, which is chosen from experimental data; for example, 2% for propane [11,12]. The soot concentration is determined from the chemical species equation (Equation (4)).

Radiation plays an important role in the combustion process. It is solved here in parallel with the governing equations. The discrete transfer method [13] is used to provide the radiation source term for the energy equation of the gas phase and the radiation flux to the solid surface. The absorption and emission of gas and soot are also considered. The effects of gas and soot on the radiation intensity are given by:

$$\frac{dI}{ds} = -(k_g + k_s)I + \frac{\sigma}{\pi}(k_g + k_s)T^4. \tag{15}$$

Scattering is negligible due to the small diameter of the soot particles. The absorption coefficients for gas and soot (Equations (16) and (17)) presented by Novozhilov et al. [14] are used, and the soot density is assumed to be 2000 kg/m^3 for the soot volume fraction (f_v) calculation [15,16].

$$k_g = 0.28 \exp\left(-\frac{T}{1135}\right) \tag{16}$$

$$k_s = 1264 f_v T. \tag{17}$$

The solution of these equations is based on the finite volume method. Convection terms are discretized using a second-order upwind differencing scheme. The SIMPLE pressure correction algorithm is used.

Firebrand Model

It is not practical to model all the physical processes of firebrand scattering at one time due to its complexity. Here its process is modeled. Firebrands are assumed to be spherical, and the behavior of firebrands in the airflow can be considered to obey an air–solid two-phase flow. Therefore, the scattering of firebrands can be presented by the Lagrangian transport equation. It is assumed that the combustion time of firebrands is much longer than the flying time, and the temperature of firebrands gives no influence on the air flow and the mass and shape are not changed during flight. From these assumptions one can obtain the following momentum equation:

$$m_d \frac{d\boldsymbol{u}_d}{dt} = \boldsymbol{F}_g + \boldsymbol{F}_{dr} + \boldsymbol{F}_p \tag{18}$$

where $\boldsymbol{F}_g = V_d(\rho_d - \rho_f)\boldsymbol{g}$ $(\boldsymbol{g} = (0,0,-9{,}8)\text{m/s}^2)$ is the force due to gravity. The drag $\boldsymbol{F}_{dr}$ is given by

$$\boldsymbol{F}_{dr} = \frac{1}{2} C_d \rho_f A_d |\boldsymbol{u} - \boldsymbol{u}_d| (\boldsymbol{u} - \boldsymbol{u}_d) \tag{19}$$

where $\boldsymbol{u}_d$ is the velocity of the firebrand, and $\boldsymbol{F}_p$ is the pressure gradient force due to the acceleration motion of the fluid [17]. This term is thought to be important because the fluid is accelerated by the thermal plume around the fire.

$$\boldsymbol{F}_p = -V_d \nabla p \tag{20}$$

The drag coefficient C_{d} is calculated using the following expression:

$$C_d = \begin{cases} 24(1 + 0.15\mathrm{Re}_d^{0.687})/\mathrm{Re}_d, & \mathrm{Re}_d \leq 10^3 \\ 0.44, & \mathrm{Re}_d > 10^3 \end{cases} \tag{21}$$

where Re_d is the Reynolds number of the firebrand.

$$\mathrm{Re}_d = \frac{\rho_{\mathrm{f}} |\boldsymbol{u} - \boldsymbol{u}_{\mathrm{d}}| D_{\mathrm{d}}}{\mu}. \tag{22}$$

The air velocity $\boldsymbol{u}$ is given by the sum of the average velocity $\tilde{\boldsymbol{u}}$ and the turbulence fluctuation $\boldsymbol{u}'$.

$$\boldsymbol{u} = \tilde{\boldsymbol{u}} + \boldsymbol{u}'. \tag{23}$$

The turbulence fluctuation is selected randomly from the Gaussian distribution probability density function with the following standard deviation σ.

$$\sigma = \sqrt{\frac{2k}{3}} \tag{24}$$

$$G(\boldsymbol{u}') = \frac{1}{\sqrt{2\pi}\sigma} \exp\left(-\frac{\boldsymbol{u}'^2}{2\sigma^2}\right) \tag{25}$$

VALIDATION OF THE CFD MODEL

The CFD model is validated by the fire wind tunnel experiment which was performed by Hayashi et al. [18] in order to study the fire plume characteristics in urban fires. Figure 2 shows the simulation domain ($4.5 \times 3.3 \times 3.0\,\mathrm{m}^3$). The burning building is represented by a propane burner ($0.3 \times 0.3 \times 0.2\,\mathrm{m}^3$). Section A–A′ is on the center line of the burner in the X-direction. The simulation cases are shown in Table 2. Table 3 shows the boundary conditions. The inflow wind velocity and turbulent intensity are set according to the experiments, and a generalized log law is used for the solid wall boundary conditions. Free-flow conditions are used for the outflow boundary conditions. The free slip condition is used for the lateral and upper boundary conditions. The boundary condition of the burning wall surface which is on fire is set to an inlet condition. Appendix A presents the calculation of the

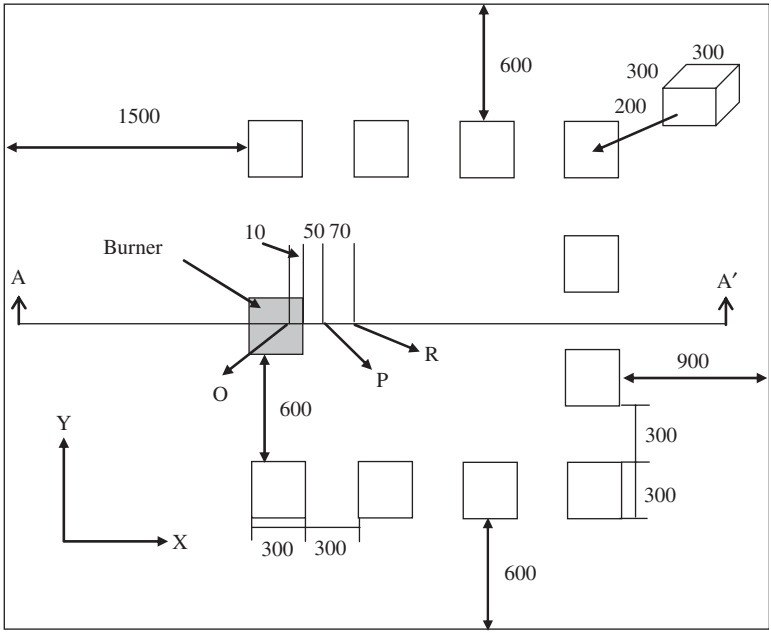

Figure 2. Simulation domain (mm).

Table 2. Simulation cases for CFD validation.

Case	Wind velocity ($Z = 0.4$ m) (m/s)	Heat release rate (kW)
1	1	15
2	2	15
3	1	26
4	2	26

inflow velocity of propane (W_z), which is perpendicular to the wall surface. The scattering of firebrands is greatly influenced by the fire source. It is very important to validate the model near the fire source. Far from the fire source, compressibility of the fluid is substantially reduced, almost to the point of becoming incompressible. The accuracy of the standard $k-\varepsilon$ model to predict incompressible fluid is widely validated by earlier research [19–21]. Therefore, the validity of the model is focused on locations close to the fire source. The authors have

Table 3. Boundary conditions.

Inlet	$U = U_D(z/z_0)^{1/3}$, $k(z) = 1.5I^2U^2$, $\varepsilon(z) = C_\mu^{3/4}k(z)^{3/2}/I(z)$, $I = 0.2 - 0.1z(0 < z < 1.8)$, $I = 0.02(z \geq 1.8)$ $I(z) = (4C_\mu k(z))^{1/2}D^{1/4}z^{3/4}/U_D[3]$, $T = 293$(K)
Outlet	Free flow
Wall	Generalized log law
Burning wall surface on fire	Inlet condition $W_z = 0.0019$ m/s (Case 1, Case 2), $I = 0.05$ $W_z = 0.0031$ m/s (Case 3, Case 4), $I = 0.05$ W_z: Vertical velocity of propane (refer to Appendix A)

made a detailed validation [22], but only some of the results are shown here due to text limitations. Figure 3(a) and (b) shows the comparison between experimental data and prediction data for points O and P (see Figure 2). The simulation results are a little lower than the experimental data. The linear assumption of $k - \varepsilon$ closure is thought to be the reason, since this leads to a lower prediction. A nonlinear model may be helpful in predicting the temperature more accurately. Another possible reason is because the thermocouple detected both radiation and conduction in the experiment. The predicted total heat flux (radiation flux and convective flux) at point R (see Figure 3) is also compared with the results of these measurements in Table 4, in which reasonable agreement can be seen. The difference comes from the simplification of soot phenomenon and the deviation of the temperature prediction. Although the model needs further improvement, it can be considered acceptable at this stage for the numerical simulation of firebrands.

MEASUREMENT OF FLUID DYNAMICS PROPERTIES OF FIREBRANDS

Firebrands have various complex shapes (spherical, cylindrical, board shape, etc.), and it is very difficult to evaluate the drag force for all shapes. Then, firebrands are assumed to be spherical and the diameter which is used in the Lagrange equation is represented by the Stokes diameter of the firebrands here. Firebrands were collected from a fire wind tunnel experiment [23] and the Stokes diameters of them are determined from their densities and the terminal velocities measured by the experiments as follows.

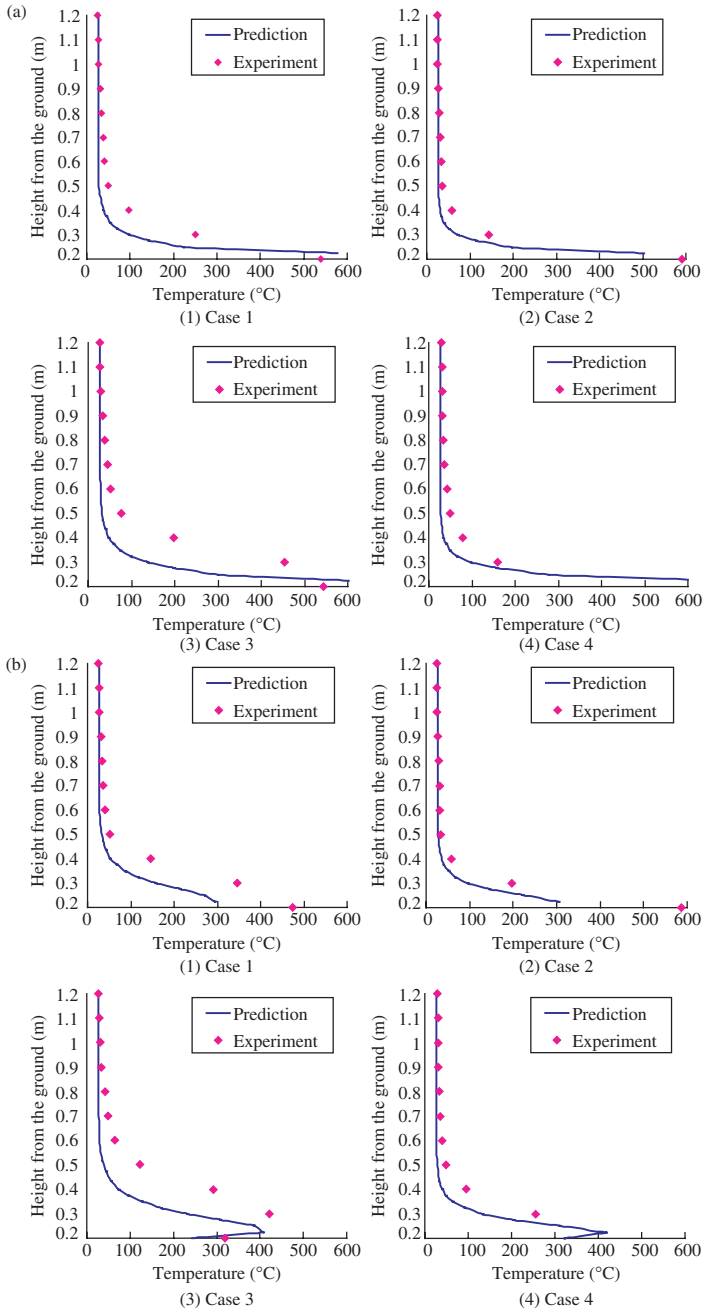

Figure 3. (a) Comparison for temperature at point O and (b) Comparison for temperature at point P.

Table 4. Comparison for total heat flux (kw/m^2).

Case	Experiment	Prediction
1	8.44	9.15
2	8.57	8.62
3	13.33	13.00
4	15.49	12.09

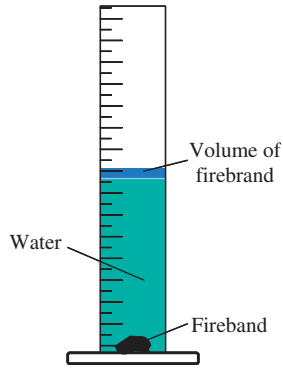

Figure 4. Measurement of volume of firebrands.

Measurement of Density

The immersion method was used to measure the densities of the firebrands. Figure 4 shows the measurement. Firebrands were immersed in water within a cylinder, from which the volume can be measured. The density was calculated from the volume and weight, which was measured using an electronic balance. Twenty pieces were measured and the average result is 130 kg/m^3 (100–180 kg/m^3).

Measurement of Stokes Diameter

The firebrands are freely dropped from a sufficient height. A scale was printed on a white board. The time taken in passing the scale was determined using a high-speed digital video camera operating at 250 frames per second. The velocity is calculated from the time and scale. The dropping height was adjusted until it reached a constant velocity, that is, the terminal velocity. Figure 5 shows the experimental scheme.

The Stokes diameter is calculated by Equation (26) based on the measured terminal velocity. Appendix B shows the derivation of this equation.

$$D_{\mathrm{d}} = \frac{0.33\rho_{\mathrm{f}} v_{\mathrm{t}}^2}{g(\rho_{\mathrm{d}} - \rho_{\mathrm{f}})}. \tag{26}$$

The firebrands were classified into four kinds of classes according to the appearance area (Class 1–4). The classification and the measurement number are shown in Table 5 and a part of the firebrands for the measurement are shown in Figure 6. Class 2 and Class 3 are classified by the differences of shapes (spherical or cylindrical) for the firebrands of the same size. The ratio of the longest side to the shortest side for Class 2 is about 1, and the ratio for Class 3 is about 2. For Class 3, they were measured twice because it was thought that the error of measurement was large because their shapes were cylindrical.

It is found that Class 1 has the highest terminal velocity, while Class 4 has the smallest. Class 2 and 3 are almost the same. The comparison of

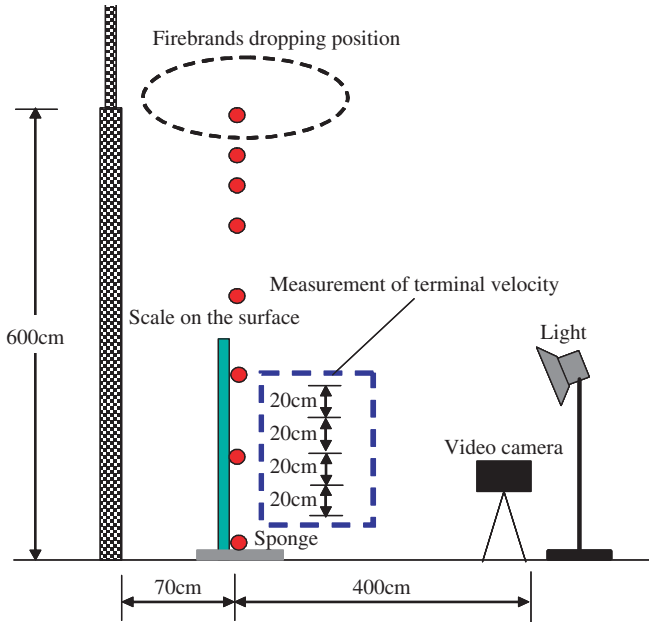

Figure 5. Firebrands dropping experiment.

Table 5. Classification of firebrands measured.

Class	Appearance area (cm^2)	Number
1	$S > 4$	27
2	$1 < S < 4$ (sphere)	46
3	$1 < S < 4$ (cylinder)	22×2
4	$1 < S$	45

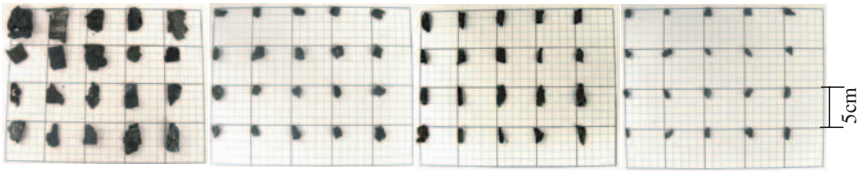

Figure 6. Classification of firebrands measured.

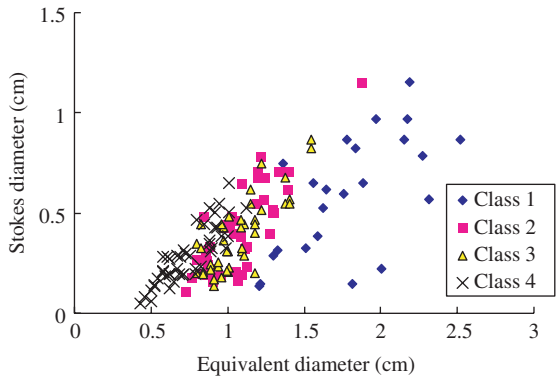

Figure 7. Comparison of equivalent diameter to Stokes diameter.

the diameter (equivalent diameter) of the firebrands when it is assumed to be spherical to the Stokes diameter is shown in Figure 7. It is concluded that the ratio of Stokes diameter to equivalent diameter is focused on 0.2–0.7 for all cases. Little difference is observed between Class 2 and Class 3 for Stokes diameters. However, it was found that the landing points on the ground are more scattered for Class 3 than Class 2, implying that differences in firebrand shapes influence not only the perpendicular direction, but also the horizontal direction.

REAL URBAN SCALE FIRE NUMERICAL SIMULATION

Real urban scale fire numerical simulations have been carried out using the numerical model and the measurement results shown above.

Simulation Conditions

Figure 8 shows the calculation area which is $X \times Y \times Z = 510 \times 110 \times 200\,\mathrm{m}^3$. The size of each building is set to be $10 \times 10 \times 10\,\mathrm{m}^3$, and the building interval is also set to be 10 m. There are fifteen buildings (5×3) and the building on fire is shown in Figure 7. The boundary conditions are shown in Table 6 and the simulation cases are shown in Table 7.

For all cases, the flow rate of the combustible gas (propane) is controlled from the burning face to get a heat release of $1.6\,\mathrm{MW/m}^2$ [3]. The inflow wind velocity is assumed 5.0 and 10.0 m/s based on the investigation of the Wakayama Shirahama Spa Fire that occurred in 1998 [1], and the wind profile is given according to the 1/4 profile for the urban area. As the firebrands (about 1 cm) are mostly generated from past investigations [1,2], the cases that the equivalent diameter is 1.0 cm and the ratio of the Stokes diameter to the equivalent diameter is 0.2–0.7 were simulated. The firebrands are assumed to be generated from 81 points averaged over the burning face, and the interval between points is 1.0 m. The firebrands with the ratio of the Stokes diameter to the equivalent diameter 0.2, 0.3, 0.4, 0.5, 0.6, and 0.7 cm are generated at the same generation ratio from generation positions. The initial

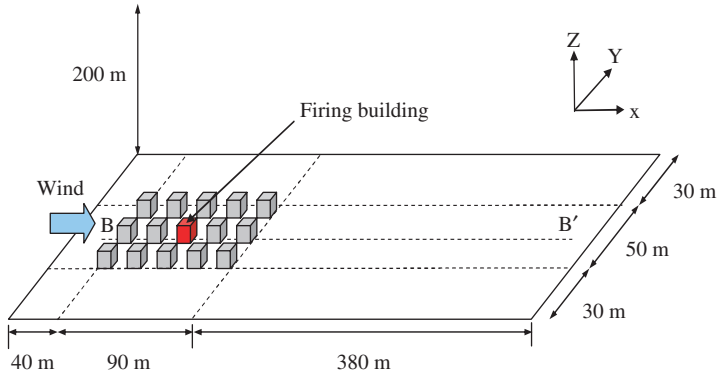

Figure 8. Analysis domain.

Table 6. Boundary conditions.

Inlet	$U = U_D(z/10)^{1/4}$, $T = 293$(K) $\varepsilon(z) = C_\mu^{3/4} k(z)^{3/2}/l(z)$ $l(z) = (4C_\mu k(z))^{1/2} D^{1/4} z^{3/4}/U_D$ [3] k: Experimental data [24]
Outlet	Free flow
Wall	Generalized log law
Burning wall surface on fire	Inlet condition $W_z = 0.018$ m/s

Table 7. Simulation cases.

Case	Inflow velocity (height 10 m) (m/s)	Burning wall on fire
1		Roof
2	5	Leeward side
3		All sides
4		Roof
5	10	Leeward side
6		All sides

*All sides include the roof.

generation velocity of the firebrands is almost not found. Here, it is thought that the generation velocity is close to the velocity of the fire plume in the top story of the building. It is reported that 5.0–10.0 Pa is the pressure difference between the fire room and the elevator shaft when the temperature is from 200 to 800°C in the building fire reported by Tamura [25]. It is assumed that the pressure difference between the fire plume and outdoor air is almost the same. Then, the velocity of the plume can be estimated to be 3.7–7.8 m/s from the Bernoulli equation ($V = \sqrt{2\Delta p/\rho}$). Here, an average value, 5.0 m/s is set to be the initial generation velocity.

RESULTS

Wind Distribution and Temperature Distribution

The vertical wind distribution and temperature distribution in the center section (Section B–B′) are shown in Figures 9 and 10.

The thermal plume is the strongest for all burning cases, the roof fire being stronger than that of the sidewall fire. The influence on the sky is small for the sidewall fire, though a strong rising flow is seen between the buildings. When the inflow wind velocity is higher, the thermal plume is suppressed and greatly inclines to the leeward side, which increases the risk of the fire spreading to neighboring buildings.

Firebrands Scattering

Figure 11 shows the firebrands scattering results. The results show that firebrands can influence a wide area in each case. For the cases of roof fires, when the inflow wind velocity is 5.0 m/s (Case 1), the firebrands

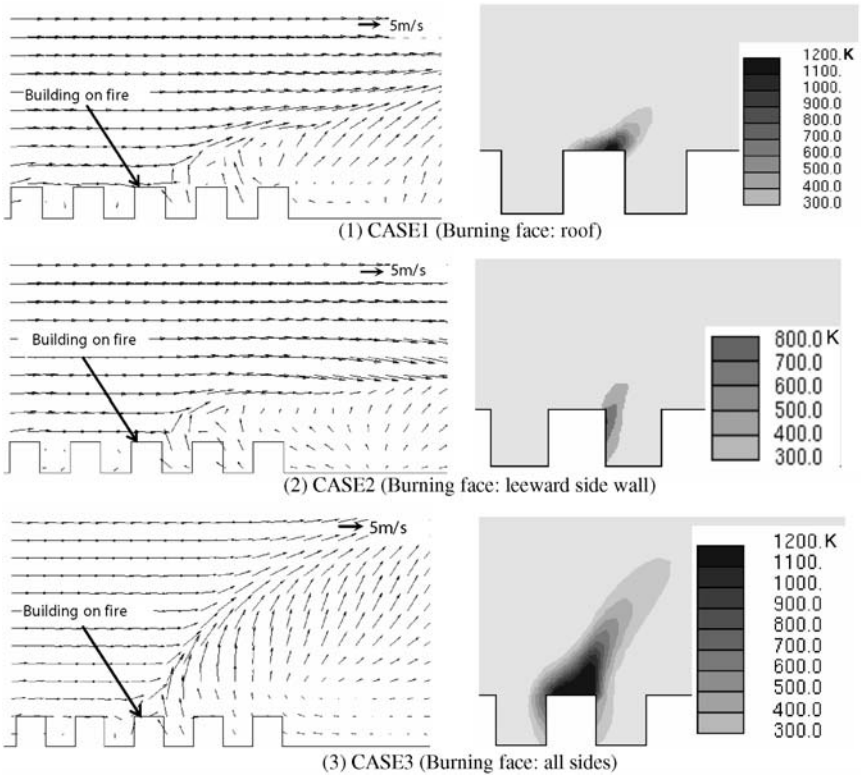

Figure 9. Vertical wind and temperature distribution (Section B–B′, inflow velocity: 5 m/s).

with a Stokes diameter of 0.2 cm can scatter 400 m or more, and the firebrands with a Stokes diameter of 0.3 cm can scatter about 100 m. The firebrands with a Stokes diameter of 0.4 cm or more almost fall down at neighboring buildings. When the inflow velocity is 10.0 m/s (Case 4), a part of the firebrands with a Stokes diameter of 0.2 cm scatter over 400 m, and the firebrands with a Stokes diameter of more than 0.3 cm all fall down at neighboring buildings. Wind velocity is strong in Case 4 compared with Case 1, so the rising flow is suppressed and scattering distances are shortened for all kinds of firebrands.

For the cases of sidewall fires, when the inflow velocity is 5.0 m/s (Case 2), the firebrands with a Stokes diameter of 0.2 cm can scatter about 200 m, and the firebrands with a Stokes diameter of 0.3 cm

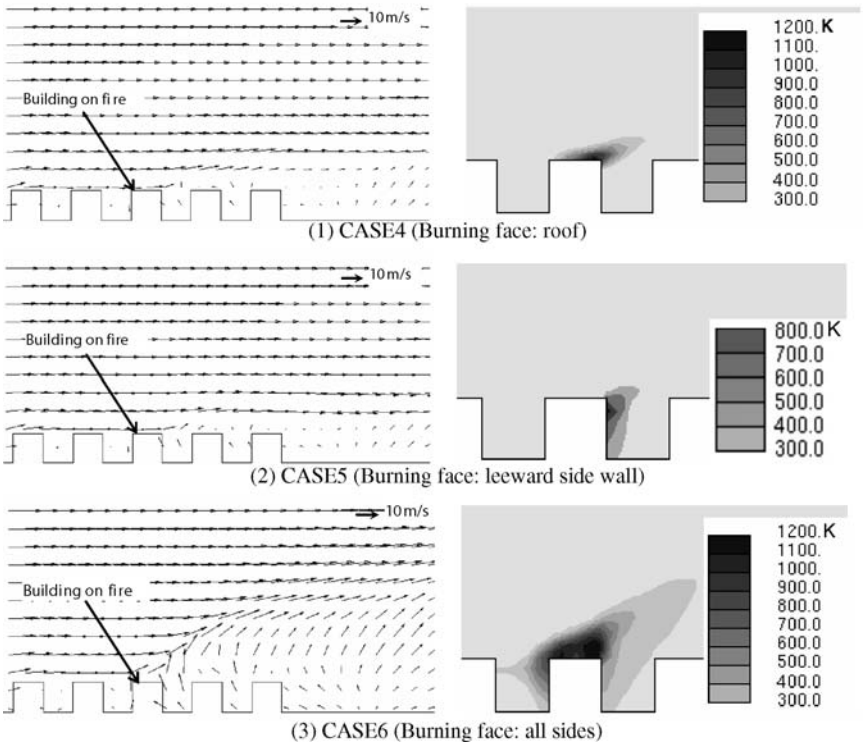

Figure 10. Vertical wind and temperature distribution (Section B–B′, inflow velocity: 10 m/s).

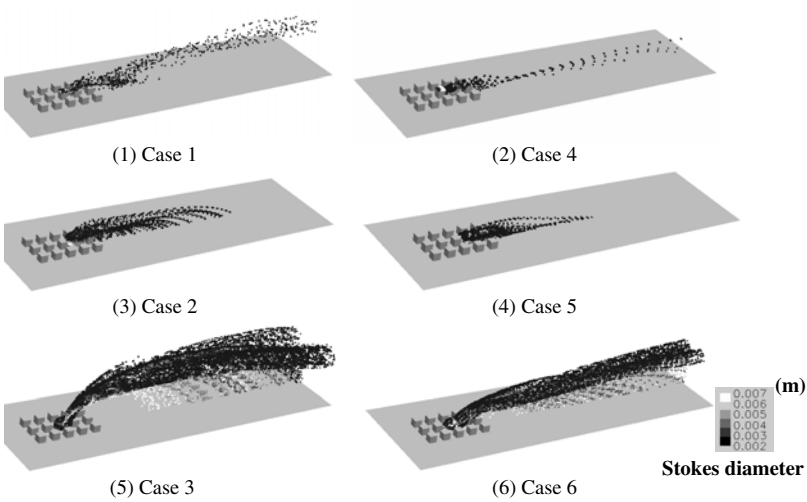

Figure 11. Firebrands trajectories.

can scatter about 100 m. The firebrands with a Stokes diameter of 0.4 cm or more almost fall down at neighboring buildings. When the inflow velocity is 10.0 m/s (Case 5), the firebrands with a Stokes diameter of 0.2 cm can scatter about 150 m, and the firebrands with a Stokes diameter of 0.3 cm can scatter about 80 m. The firebrands with a Stokes diameter of 0.4 cm or more almost fall down at neighboring buildings. The rising flow for Case 5 is weaker than that for Case 2 that the inflow wind velocity is low and scattering distances are shortened for all kinds of firebrands.

For the all side burning cases, all kinds of firebrands scatter over 100 m due to the rising flow. Compared with Case 3 (inflow wind velocity: 5.0 m/s), the scattering distances increase for Case 6 (inflow wind velocity: 10.0 m/s). This is because the rising flow in Case 6 is a little weaker, the firebrands can be raised up to the sky due to the rising flow, then follow the wind in the sky which is stronger in Case 6.

CONCLUSIONS

In order to simulate urban fire and firebrands behavior, the CFD model, combustion model, radiation model, and firebrands scattering model

have been coupled. The Stokes diameter and density of the firebrands which are necessary in the firebrands scattering model were measured. The ratio of the Stokes diameter to the equivalent diameter is focused on 0.2–0.7. An urban fire simulation in a modeled urban area has been conducted using the coupled model and the firebrand experimental data. It is found that when the inflow wind velocity is comparatively slow, the size of the thermal plume becomes significant, and when the inflow wind velocity is high, the thermal plume is suppressed and greatly inclines to the leeward side, which increases the risk of the fire spreading to neighboring buildings. The scattering of the firebrands that the combustion time is longer enough than the flying time is analyzed. The firebrand can scatter over a wide area, more than 400 m. It is also shown that the scattering distance is strongly influenced by whether the firebrands can be raised up by the rising flow and follow the urban wind in the sky.

NOMENCLATURE

A_d = firebrand cross-sectional area (m^2)
C_d = drag coefficient
C_p = specific heat (J/kg/K)
C_μ = constant in the $k-\varepsilon$ model
$C_{\varepsilon i}$ = constant in the $k-\varepsilon$ model
D = typical scale (m)
D_d = firebrand diameter (m)
D_n = molecular diffusion coefficient of nth species (m^2/s)
$\bar{f}$ = Reynolds average of variable f
$\tilde{f}$ = Favre average of variable f
$\boldsymbol{F}_{dr}$ = drag (N)
$\boldsymbol{F}_p$ = pressure gradient force due to the acceleration motion of the fluid (N)
$\boldsymbol{F}_g$ = gravity (N)
f_v = soot volume fraction
h = enthalpy (J/kg)
$h_{0,n}$ = standard formation enthalpy (J/kg)
h_n = enthalpy of nth species (J/kg)
I = radiative intensity ($J/m^2/s$)
k = turbulent kinetic energy (m^2/s^2)
k_g = gas absorption
k_s = soot absorption
l = turbulent scale (m)

L = model scale
m_{d} = firebrand mass (kg)
M_n = molecular weight of nth species
P = pressure (Pa)
Re_d = Reynolds number of firebrand
S = soot conversion factor, or distance along the radiation ray (m)
S_{R} = radiative heat source (W/m^3)
t = time (s)
T = temperature (K)
u_{d} = firebrand velocity (m/s)
u_i = three components of velocity (m/s) ($u_1 = U_1$: velocity in direction of main flow, $u_2 = U_2$: velocity in horizontal direction, and $u_3 = \mathrm{U}_3$: velocity in vertical direction)
U_{D} = inflow wind velocity (m/s)
V_{d} = volume of firebrand
v_{t} = terminal velocity of firebrand (m/s)
W_z = inflow velocity of fuel (m/s)
x_i = three components of spacial coordinate ($x_1 = X$: main flow direction, $x_2 = Y$: horizontal direction, and $x_3 = Z$: vertical direction)
Y_n = mass fraction of nth species

Greek Symbols

ε = turbulent kinetic energy dissipation rate (m^2/s^3)
λ = thermal conductivity (W/m/K)
μ = viscosity (kg/m/s)
μ_{t} = turbulent viscosity (kg/m/s)
ρ = density (kg/m^3)
ρ_{d} = density of firebrand (kg/m^3)
ρ_{f} = density of air (kg/m^3)
σ = Stefan–Boltzmann constant 5.67×10^{-8} (W/m^2/K^4) or standard deviation
σ_{h} = turbulent Prandtl number
σ_n = turbulent Schmidt number
σ_k = constant in the $k-\varepsilon$ model
σ_ε = constant in the $k-\varepsilon$ model
τ_{ij} = viscous stress tensor (N/m^2)
w_n = chemical reaction rate of nth species (kg/m^3/s)

ACKNOWLEDGMENTS

The authors would like to express thanks to Dr Yoshifumi Omiya (Tokyo University of Science) and Dr Tatsuya Iwami (National Institute for Land and Infrastructure Management) for their valuable advice.

APPENDIX A

The boundary condition of the burning wall surface which is on fire is set to the inlet condition. W_z means the inflow velocity of propane perpendicular to the wall surface. It is decided as follows:

It is known that

$$Q = \rho_{C3H8} W_z A \Delta H_C$$

where Q is the heat release rate (kW); ρ_{C3H8} is the density of propane (1.9 kg/m^3); A is the area of burning wall surface (m^2); and ΔH_C is the heat of combustion of propane (46,460 kJ/kg).

Then, W_z is calculated from the heat release rate. For example, when Q is 15 kW, then W_z is 0.0019 m/s.

APPENDIX B

Equation (26) was derived as follows:

When the firebrands are at terminal velocity, then

$$\boldsymbol{F}_g = -\boldsymbol{F}_{dr}$$

$$V_d(\rho_d - \rho_f)g = \frac{1}{2} C_d \rho_f A_d v_t^2$$

$$\frac{1}{6}\pi D_d^3(\rho_d - \rho_f)g = \frac{1}{2} C_d \rho_f \frac{1}{4}\pi D_d^2 v_t^2$$

The value, 0.44 is used for Cd due to the high Reynolds number (>1000). Then,

$$D_d = \frac{0.33 \rho_f v_t^2}{g(\rho_d - \rho_f)}$$

REFERENCES

1. Ohmiya, Y. and Iwami, T. (1999). An Investigation on the Distribution of Firebrands and Spot Fires in a Hotel Fire, *AIJ Journal of Technology and Design*, **9**: 133–136 (in Japanese).
2. Iwami, T. and Koji, K. (2002). Report on City Fire in Wakkanai – Part 2, State of Damaged Buildings and Distribution of Firebrands in the Surrounding Area, *Fire*, **52**: 51–53 (in Japanese).
3. Shiraishi, Y., Kato, S., Yoshida, S. and Murakami, S. (2001). Numerical Analysis of Scatter of Firebrands within Urban Fire Spread, *Journal of Architecture, Planning and Environmental Engineering*, **546**: 187–192 (in Japanese).
4. Hayashi, Y., Ohmiya, Y., Iwami, T., Kakei, M., Goto, N. and Saga, T. (2003). Numerical Analysis of Scatter of Firebrands, *AIJ Journal of Technology and Design*, **17**: 203–208 (in Japanese).
5. Huang, H., Ooka, R., Kato, S., Otake, H. and Hayashi, Y. (2004). CFD Simulation of Thermal Plume and Firebrands Scattering in Urban Fire, *Fire Science and Technology*, **23**(2): 152–163.
6. Himoto, K. and Tanaka, T. (2005). Transport of Disk-shaped Firebrands in a Turbulent Boundary Layer, *8th International Symposium on Fire Safety Science*, pp. 433–444.
7. EI Tahry, S.H. (1983). k-ε Equation for Compressible Reciprocating Engine Flows, *AIAA J Energy*, **7**(4): 345–353.
8. Magnussen, B.F. and Hjertager, H. (1976). On Mathematical Modeling of Turbulent Combustion with Special Emphasis on Soot Formation and Combustion, In: *Proceeding of 16th Symposium (International) on Combustion*, The Combustion Institute, pp. 719–729.
9. Bilger, R.W. (1995). Computational Field Models in Fire Research and Engineering, In: *Proceeding of 4th Symposium (International) on Fire Safety Science*, The Combustion Institute, pp. 95–110.
10. Novozhilov, V., Moghtaderi, B., Fletcher, D.F. and Kent, J.H. (1996). Computational Fluid Dynamics Modeling of Wood Combustion, *Fire Safety Journal*, **27**: 69–84.
11. Yan, Z.H. and Holmstedt, G. (1996). CFD and Experimental Studies of Room Fire Growth on Wall Lining Materials, *Fire Safety Journal*, **27**: 201–238.
12. Tewarson, A. (1995). Generation of Heat and Chemical Compounds in Fires, *The SFPE Handbook of Fire Protection Engineering*, **2nd edn**, Chapters 3–4.
13. Lockwood, F.C. and Shah, N.G.A. (1981). New Radiation Solution Method for Incorporation in General Combustion Prediction Procedures, In: *Proceeding of 18th Symposium (International) on Combustion*, The Combustion Institute, pp. 1405–1414.
14. Novozhilov, V., Harvie, D.J.E., Kent, J.H., Apte, V.B. and Pearson, D.A. (1997). Computational Fluid Dynamics Study of Wood Fire Extinguishment by Water Sprinkler, *Fire Safety Journal*, **29**: 259–282.

15. Jia, F., Galea, E.R. and Patel, M.K. (1998). The Numerical Simulation of Fire Spread within a Compartment using an Integrated Gas and Solid Phase Combustion Model, *Journal of Applied Fire Science*, **8**(4): 327–352.
16. Fairweather, M., Jones, W.P. and Lindstedt, R.P. (1992). Predictions of Radiative Transfer from a Turbulent Reacting Jet in a Crosswind, *Combustion and Flame*, **89**: 45–63.
17. Hinze, J.O. (1975). *Turbulence*, pp. 460–471, McGraw-Hill, New York.
18. Hayashi, Y., Saga, T., Suzuki, K. and Wakamatsu, T. (2002). Study on Flames and Thermal Plumes Induced by Fires under Windy Conditions, *Summaries of Technical Papers of Annual Meeting of Architectural Institute of Japan*, pp. 297–300 (in Japanese).
19. Murakami, S. (1990). Numerical Simulation of Turbulent Flow Field Around Cubic Model Current Status and Applications of k-ε Model and LES, *Journal of Wind Engineering and Industrial Aerodynamics*, **33**: 139–152.
20. Huang, H., Ooka, R. and Kato, S. (2005). Urban Thermal Environment Measurements and Numerical Simulation for an Actual Complex Urban Area Covering a Large District Heating and Cooling System in Summer, *Atmospheric Environment*, **39**: 6362–6375.
21. Huang, H., Akutsu, Y., Arai, M. and Tamura, M. (2000). A Two-dimensional Air Quality Model in an Urban Street Canyon: Evaluation and Sensitivity Analysis, *Atmospheric Environment*, **34**: 689–698.
22. Otake, H., Huang, H., Ooka, R., Kato, S. and Hayashi, Y. (2004). Simulation of Flames and Thermal Plume in Urban Fire under Windy Condition, *Journal of Institute of Industrial Science*, **56**:11–16 (in Japanese).
23. Yoshioka, H., Hayashi, Y., Omiya, Y., Noguchi, T., Kato, S. and Ooka, R. (2003). Full-scale Fire Wind Tunnel Experiments on Generation of Firebrands from a Burning House, *Summaries of Technical Papers of Annual Meeting of Architectural Institute of Japan*, pp. 117–118 (in Japanese).
24. Murakami, S., Mochida, A. and Hayashi, Y. (1988). Modification of Production Terms in k-ε Model to Remove Overestimate of k Value Around Windward Corner, *10th Wind Engineering Symposium*, pp. 199–204 (in Japanese).
25. Tamura, G.T. (1994). *Smoke Movement and Control in High-rise Buildings*, The National Fire Protection Association, Quincy, Massachusetts.

BIOGRAPHIES

Hong Huang

Dr Hong Huang has a PhD degree in Chemical Engineering from the University of Tokyo, Japan (2000). He is a research associate in the Institute of Industrial Science, The University of Tokyo. His research is focused on the numerical simulation and wind tunnel experiment of fire

spread and smoke movement. He is a member of the Architecture Institute of Japan.

Ryozo Ooka

Dr Ryozo Ooka is an associate professor of the Institute of Industrial Science, The University of Tokyo. He has a PhD degree in Architecture from the University of Tokyo, Japan (1997). His research areas are numerical simulation of thermal plume, fire engineering, etc. He is a member of the Architecture Institute of Japan.

Shinsuke Kato

Dr Shinsuke Kato is a professor of the Institute of Industrial Science, The University of Tokyo. He received PhD degree in Architecture from the University of Tokyo, Japan (1980). His research interest areas are smoke and fire control in rooms, airflow and temperature distributions in rooms, etc. He is a member of Architecture Institute of Japan.

Yoshihiko Hayashi

Dr Yoshihiko Hayashi is a chief researcher in the Building Research Institute of Japan with many years of experience in the fire tunnel experiment and numerical simulation. He is a member of the Architecture Institute of Japan.